DOI: 10.1002/ejic.200900882

Template-Free Synthesis of Magnetic Chains Self-Assembled from Urchin-Like Hierarchical Ni Nanostructures

Lu-Ping Zhu,*[a] Gui-Hong Liao,[b] Wei-Dong Zhang,[b] Yang Yang,[b] Ling-Ling Wang,[a] and Hong-Yong Xie[a]

Keywords: Nanostructures / Hydrothermal method / Ferromagnetism / Self-assembly / Nickel

Magnetic chains self-assembled from urchin-like hierarchical Ni nanostructures have been successfully synthesized by a simple hydrothermal method requiring 4 h at 115 °C without any template or surfactant. The individual urchin-like hierarchical nanostructures have an average diameter of 2–4 μm and are composed of well-aligned sword-like nanopetals growing radially from the surfaces of the spherical particles. The products were characterized by means of X-ray powder diffraction (XRD), scanning electron microscopy (SEM), transmission electron microscopy (TEM), energy-dispersive X-ray spectroscopy analysis (EDX), Fourier transform infrared (FTIR) spectroscopy, thermogravimetric and differential scanning calorimetric analysis (TGA-DSC). A rational formation mechanism of magnetic chains was proposed. Magnetic hysteresis measurements revealed that the as-synthesized Ni chain-like architectures display ferromagnetic behavior with saturation magnetization, remanent magnetization, and coercivity values of 52.58 emu/g, 5.82 emu/g, and 211.67 Oe, respectively.

Introduction

It is believed that the properties of nanomaterials strongly depend on their size, shape, and dimensionality.[1] In recent years, there has been great interest in the synthesis of nanomaterials with various architectures, because of their potential applications in optics, electronics, magnetism, and biology.[2] Remarkable progress has been made in the self-assembly of highly organized building blocks of metals,[3] semiconductors,[4] copolymers,[5] organic–inorganic hybrid materials,[6] and biomaterials[7] based on different driving mechanisms. However, since the self-assembly process is considerably complex, it is still a big challenge to develop simple and reliable synthetic methods for hierarchically self-assembled architectures with novel and interesting morphologies, which would lead to novel properties of micro-/nanomaterials.

As an important material displaying magnetic anisotropy, nickel has also attracted much attention and has been the focus of intense research. Various Ni micro/nanostructures, such as nanocrystals,[8] nanorods,[9] nanoneedles,[10] nanochains,[11] nanobelts,[12] nanotubes,[13] nano-/submicrometer hollow spheres,[14] microwires,[15] nanofibers,[16] and nanosheets[17] have been successfully synthesized by different methods. Since ordered micro/nanostructures have potential application in catalysts, magnetic recording, and drug delivery because of their dimensions and morphologies, the synthesis of nickel hierarchical architectures is desirable. Zheng et al. synthesized nickel nanocrystals with distinct flower shapes by reduction of the mixed complexes of $Ni(N_2H_4)_3^{2+}$ and $Ni(dmg)_2$ (nickel dimethylglyoximate) in alkaline solution with hydrazine hydrate.[18] Fu and coworkers prepared Ni dendritic nanostructures by a hydrothermal reduction approach in the presence of the surfactant CTAB.[19] Very recently, the self-assembly of Ni nanopetals into dandelion/urchin-like three-dimensional nanostructures by a solvo-/hydrothermal route was reported.[20] However, to the best of our knowledge, the synthesis of Ni chain-like architectures consisting of urchin-like hierarchical nanostructures has not been reported until now.

In our previous work, we reported the synthesis of chain-like ferromagnetic CoNi alloy particles, Co dendritic superstructures and flower-like hierarchical microspheres using wet-chemical methods.[3c,3d,21] Herein, we report the facile synthesis of Ni chain-like architectures consisting of urchin-like hierarchical nanostructures by an ethylenediamine (EDA)-assisted self-assembly process. The chain-like architectures can be expected to bring about new opportunities in research and application as catalysts and other related micro- and nanodevices. We have proposed a possible formation mechanism for the Ni chains self-assembled from urchin-like hierarchical nanostructures.

Results and Discussion

The phase structure and purity of the as-synthesized samples were examined by XRD. The XRD pattern of the

[a] School of Urban Development and Environmental Engineering, Shanghai Second Polytechnic University, Shanghai, 201209, China
E-mail: lpzhu@mail.ipc.ac.cn; lpzhu@eed.sspu.cn
[b] Technical Institute of Physics and Chemistry, Chinese Academy of Sciences, Beijing 100190, China

as-obtained products is shown in Figure 1. Three characteristic peaks can be indexed as the (111), (200), and (220) planes of the face-centered cubic (fcc) phase Ni, which is in agreement with reported data (JCPDS: No. 04-0850). No characteristic peaks due to the impurities of nickel oxides or hydroxides were detected, indicating that the as-obtained product was pure. Considering the presence of hydrazine hydrate and the release of N_2 when the reaction was carried out, it is not difficult to understand this.

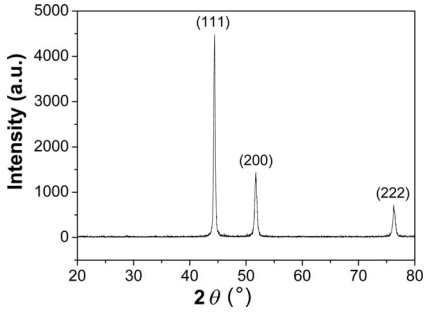

Figure 1. XRD pattern of the as-synthesized Ni architectures treated at 115 °C for 4 h.

The morphology and dimensions of the as-prepared products were examined by SEM (Figure 2). Figure 2(a) shows the panoramic morphology of the samples, which indicates that the as-obtained products consist of large-scale chain-like structures composed of relatively uniform spheres with an average diameter of 2–4 μm. These chain-like assemblies with many branches range from several microns to dozens of microns in size and are present in high quantity. In fact, it is hard for us to discern where the chains end, because they are almost intertwined with each other. The SEM image at a higher magnification shown in Figure 2(b) displays the detailed structure of the chain-like architectures assembled from urchin-like hierarchical nanostructures. A partially magnified view of the samples indicates that the urchin-like hierarchical nanostructures comprise dozens of sword-like petals radiating from the center [see Figure 2(c)]. The petals with sharp ends and protruding surface ridges have sizes in the range 200–400 nm in diameter, 100–200 nm in thickness, and 0.5–1.2 μm in length. It is noteworthy that the chains as well as the urchin-like hierarchical nanostructures show considerable stability and they maintain their structure even after 30 min of ultrasonication. Figure 2(d) shows a representative EDX spectrum of Ni chain-like architectures, which indicates that the sample is essentially pure Ni. In order to confirm this result, the products were investigated with TGA-DSC measurements. As shown in the inset in Figure 2(d), the as-synthesized nickel products began to be oxidized (weight gain) at around 250 °C and were fully oxidized at around 700 °C. The final weight gain was around 27.0%, which was almost consistent with the theoretical weight gain (27.3%) for the perfect conversion of pure Ni to NiO. Both the EDX and TGA analyses demonstrate that a pure metallic Ni product could be obtained under the current synthesis conditions and the Ni chain-like architectures were very stable in ambient atmosphere; this is consistent with both the XRD and the results reported in the literature.[12] The DSC curve shows an exothermic peak with a maximum located at ca. 585 °C. The temperature range of the exothermic peak in the DSC curve fits well with that of the weight gain in the TGA curve, corresponding to exothermic behavior during the oxidation of Ni to NiO.

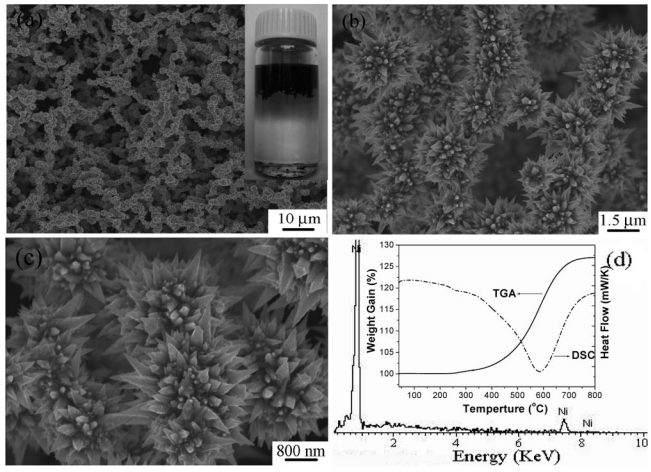

Figure 2. SEM images of the Ni chains self-assembled from urchin-like hierarchical nanostructures synthesized by hydrothermal treatment at 115 °C for 4 h. (a) The low-magnification SEM image; the inset is the photograph of the as-prepared Ni chain-like architectures in the mother liquor. (b) and (c) The high-magnification SEM images. (d) The EDX spectrum; the inset in (d) shows the corresponding TGA-DSC curve.

The chain-like structure of the products was further examined by TEM and HRTEM studies. Figure 3(a) shows a representative TEM image of the as-synthesized nickel samples. It can be seen that the chain-like architectures consist of urchin-like hierarchical nanostructures, agreeing well with the SEM observations. Figure 3(b) is the enlarged TEM image of the edge area of an individual Ni urchin-like hierarchical nanostructure [from Figure 3(a)]. Sword-like petals radiating from the spherical particles can be seen clearly, which is consistent with the SEM results shown in Figure 2. Figure 3(c) is the corresponding selected area electron diffraction (SAED) pattern of a sword-like petal [Figure 3(b)]. The SAED pattern exhibits a regular and clear diffraction spot array, which illustrates the single crystal nature of the sword-like petal. Figure 3(d) is a HRTEM image of the part of a typical sword-like petal enclosed in a box in Figure 3(b). The lattice interplanar spacing is measured to be ca. 0.20 nm, which corresponds to the (111) plane of the fcc Ni metal. Both the HRTEM image and the SAED pattern indicate that the sword-like petal of Ni metal grows in the [011] direction, which agrees well with the XRD result. In addition, a kind of outer shell of a different material in this petal can be observed from Figure 3(d). It is well known that EDA can be employed as a capping agent and shape controller in the synthesis of nanoparticles.[22–29] Therefore, the material forming this outer shell may be the EDA that has not been removed by washing.

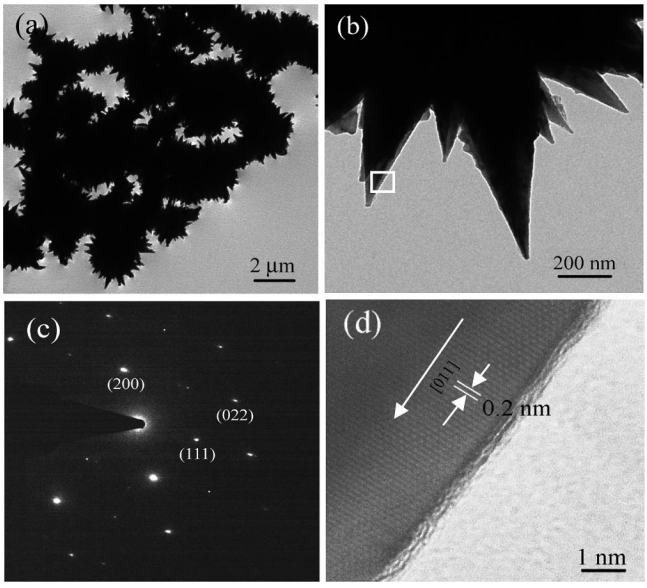

Figure 3. (a) and (b) TEM images of the as-synthesized Ni architectures treated at 115 °C for 4 h. (c) SAED pattern of one petal taken from the urchin-like Ni hierarchical nanostructures. (d) HRTEM image for the area enclosed in a box in (b).

To investigate the growth process of the Ni chain-like architectures in detail, we studied the structure and morphology evolution of the product with SEM and XRD at different growth stages of the hydrothermal process. As shown in Figure 4(a), in the early stage, spherical nickel particles with diameters of about 1–2 μm emerged as the initial product. The surfaces of the as-synthesized nickel particles are quite smooth. After a reaction time of 1 h, short sword-like petals began to grow out of these spherical particles, and some particles developed into chain-like architectures assembled from deficient urchin-like nanostructures, as shown in Figure 4(b), indicating that self-assembly was still under way. After a reaction time of 2 h, most of the product had evolved into chain-like architectures assembled from urchin-like nanostructures at an early stage of development, as shown in Figure 4(c). The length of the sword-like petals is about 500 nm. After a reaction time of 4 h, all of the products had evolved into chain-like architectures assembled from fully developed urchin-like nanostructures, as shown in Figures 4(d) and 2. It is notable that besides chain-like architectures assembled from fully developed urchin-like nanostructures, some microwires with hierarchical nanostructures were also observed [inset in Figure 4(d)], which may be caused by the tight attachment of adjacent urchin-like nanostructures. This result indicates that it would not be possible to distinguish the boundary between two urchin-like nanostructures after a certain reaction time. The corresponding XRD patterns of the Ni samples obtained at different time intervals are shown in Figure 5. Notably, when the reaction time was prolonged, the intensity of all the peaks belonging to the Ni fcc phase increased, suggesting that the longer reaction time favors the crystallization of the Ni phase. The corresponding full width at half-maximum (FWHM) of the reflections decrease gradually with the increase in reaction time. According to the Scherrer formula:[30] $D = k\lambda/(\beta\cos\theta)$ (where D is the average dimension of particles, K is the Scherrer constant, and β is the FWHM of a reflection), the above-mentioned result indicates that the average grain diameter of the as-obtained particles increases gradually, which is consistent with the SEM results shown in Figure 4.

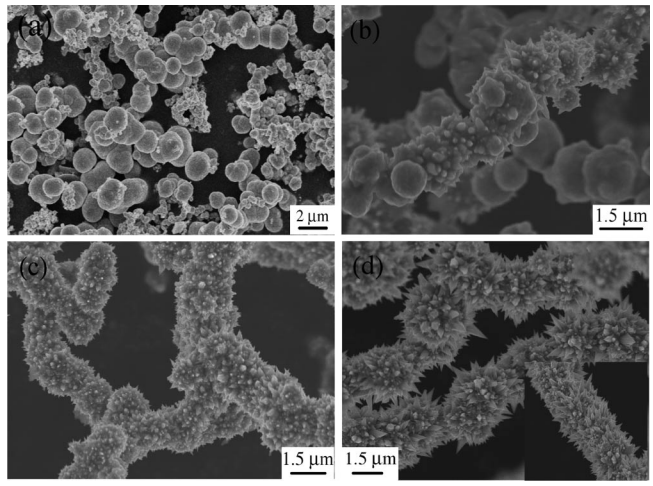

Figure 4. SEM images of the as-synthesized Ni samples collected at different intervals after the appearance of the precipitate: (a) 0.5 h, (b) 1 h, (c) 2 h, and (d) 4 h.

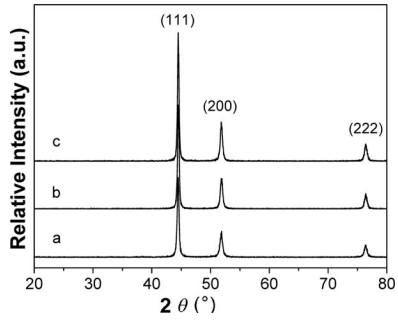

Figure 5. XRD patterns of the as-prepared samples at various growth stages of the hydrothermal process: (a) 0.5 h, (b) 1 h, and (c) 2 h.

Apart from the reaction time, EDA, which is an important ligand for metal ions and has been widely employed as a shape controller and stabilizer in the synthesis of Fe_3O_4 hollow microspheres,[22] fine handkerchief-like Ni and NiCo nanoalloys,[23] ZnSe flower-like nanoarchitectures,[24] hollow CdS nanoboxes,[25] hexagonal, star-shaped and snowflake-shaped Cu structures,[26] dendrite-like SnS,[27] nanorods and flower-like ZnO structures,[28] and submicrometer-sized Cu and Ag crystallites,[29] has a significant effect on the formation, morphology, and structure of the as-obtained Ni products. We have systematically investigated the effect of different amounts of EDA in the range 0–8 mL. SEM images of the products prepared with different amounts of EDA are shown in Figure 6. When no EDA is added, the products take on an irregular congeries accompanied by a few hexagonal discs [Figure 6(a)]. With

0.5 mL EDA, undeveloped urchin-like spheres as well as irregular nanosheets are obtained [Figure 6(b)]. With 1.5 mL EDA, a high yield of uniform magnetic Ni chain-like architectures assembled from urchin-like hierarchical nanostructures can be obtained, as shown in Figures 2 and 3. When the amount of EDA was increased to 2.0 mL, some separate urchin-like hierarchical nanostructures could also be observed in addition to chain-like architectures [Figure 6(c)]. When the amount of EDA was increased to 4.0 mL or more, separate urchin-like hierarchical nanostructures were obtained as the dominant product [see Figure 6(d)]. These results indicate that the amount of EDA plays an important role in determining the morphology of the products. In general, a relatively high amount of EDA does not favor formation of chain-like architectures but causes formation of dispersive urchin-like nanostructures. We also tested effects of other synthetic parameters, such as the amount of ethanol, on the morphology of the product and found that ethanol is also an important factor in determining the shape of the final product. For example, when ethanol is replaced by deionized water while other parameters are kept unchanged, neither chain-like architectures nor urchin-like nanostructures can be obtained, only Ni microrods and nanoparticles are observed, as shown in Figure 6(e). On the basis of the literature[22–29] and the investigations described above, we believe that EDA plays two major roles in our system. On the one hand, EDA can coordinate with nickel ions to form $[Ni(EDA)_3]^{2+}$ complexes, which can decrease the free Ni^{2+} concentration in solution and result in the slow generation of Ni nanoparticles. Reaction velocity can be adjusted through the complexation slow-release method, which can regulate the kinetics of nucleation and growth of the products and further efficiently control the morphology and structure of the final products. On the other hand, EDA can also serve as a shape modifier and controller, which may bind to certain crystal faces of the nickel particles through its $–NH_2$ function. The FTIR spectrum of the sample [Figure 6(f)] exhibits characteristic absorptions at 1635.4 cm^{-1} (δ_{NH}) and 3473.3 cm^{-1} (ν_{NH}), which are shifted to lower frequencies relative to those of free EDA, denoting some interaction between metal and ligand. The interaction between metal and ligand could force the nanoparticles to be assembled. Such a role of EDA has been reported in the literature.[22–29] Thus, the formation of the Ni chain-like architectures consisting of urchin-like hierarchical nanostructures in hydrothermal conditions would result from nucleation and continuous assembly through an oriented-attachment mechanism[31] assisted by EDA.

On the basis of previous studies of nickel/cobalt nanostructures from different complexes[3c,11,12,18] and the above results of the present study, we believe that EDA and reaction time play important roles in the formation of chain-like hierarchical architectures. A possible formation process involving the nucleation-assembly-further growth mechanism is schematically illustrated in Figure 7. The chemical reaction in the process to obtain Ni chain-like hierarchical architectures could be formulated as follows:

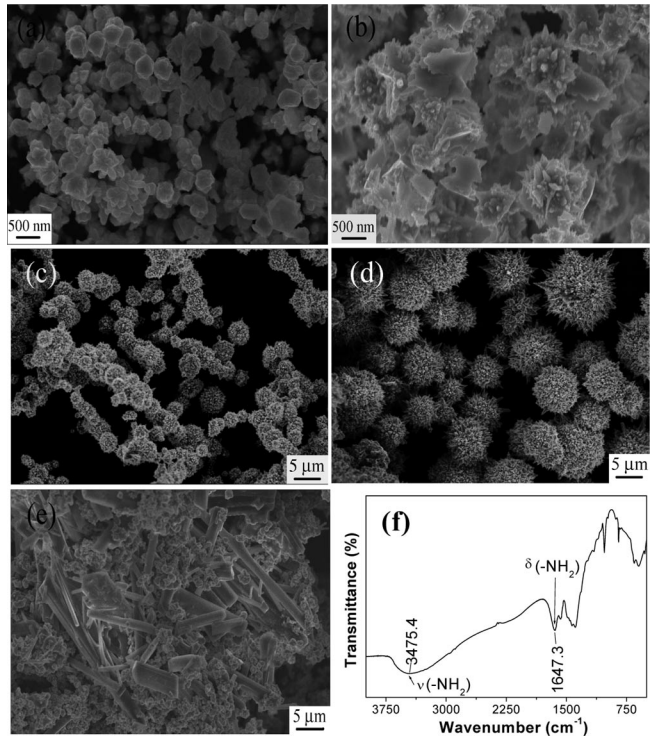

Figure 6. SEM image of Ni particles obtained with various amounts of EDA: (a) 0 mL, (b) 0.5 mL, (c) 2.0 mL, (d) 4.0 mL, (e) 1.5 mL and without ethanol, and (f) FTIR spectrum of the Ni samples hydrothermally treated in the presence of 1.5 mL EDA at 115 °C for 4 h and unwashed before measurement.

$$Ni^{2+} + 3EDA \rightarrow [Ni(EDA)_3]^{2+} \quad (1)$$

$$2[Ni(EDA)_3]^{2+} + N_2H_4 + 4OH^- \rightarrow 2Ni\downarrow + 6EDA + N_2\uparrow + 4H_2O \quad (2)$$

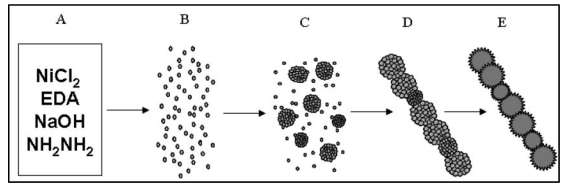

Figure 7. Schematic illustration of the formation process of the chain-like Ni architectures assembled from urchin-like hierarchical nanostructures.

In the beginning (step A), Ni^{2+} in solution reacts first with EDA to form a relatively stable complex, $[Ni(EDA)_3]^{2+}$, because of its strong affinity to Ni^{2+} at room temperature. Afterwards, in basic solution, the complex is treated with N_2H_4 causing Ni nucleation and release of EDA by a hydrothermal process (step B). The freshly crystalline nanoparticles are unstable because of their high surface energy and tend to aggregate and form larger micro/mesospheres (step C); this process is driven by the minimization of interfacial energy. Accompanied by the formation of Ni micro/nanoparticles is the magnetic dipole–dipole attraction between them. The larger Ni micro/nanoparticles were then assembled into chain-like assemblies (step D) because of the stronger anisotropic magnetic forces[11] and the

effects of EDA. This process is possible only when the magnetization of the particle does not fluctuate during the time of magnetic interaction in the suspension.[32] After the formation of chain-like structures, the micro/mesospheres that had assembled into the chain structures continued the oriented attachment process by combining with the remaining primary particles in the presence of the released EDA, finally forming the chain-like hierarchical architectures assembled from urchin-like nanostructures (step E). In our synthesis, EDA serves as ligand and shape inducer. The formation of the $[Ni(EDA)_3]^{2+}$ complex sharply decreased the free Ni^{2+} concentration in the solution, which resulted in a relatively low reaction rate of Ni^{2+} ions with N_2H_4 and OH^- ions. A slow reaction rate caused the separation of nucleation and growth steps, which is crucial for high-quality crystal synthesis. The EDA decomposed from $[Ni(EDA)_3]^{2+}$ can act as quasi-surfactants/templates to induce the further growth and assembly of nanoparticles into sword-like petals on the micro/mesosphere surfaces. The sword-like petals could organize so well that they exhibited the features of single crystals, as shown in Figure 3(c) and (d). Our time-dependent experiments support the nucleation-assembly-further growth mechanism suggested above; it was determined that the assembly process occurs after the formation of the chain-like architectures.

Magnetic measurements of the as-synthesized nickel chain-like architectures were carried out at room temperature in an applied magnetic field sweeping from –10 to 10 kOe. The hysteresis loop of the nickel chain-like architectures consisting of urchin-like hierarchical microspheres is shown in Figure 8. The inset in Figure 8 shows the magnified hysteresis loop at low applied field. The sample shows hysteresis behavior, revealing that the nickel chain-like architectures are ferromagnetic. The saturation magnetization (M_s), remanent magnetization (M_r), and coercivity (H_c) for the sample are 52.58 emu/g, 5.82 emu/g, and 211.67 Oe, respectively. Compared to the coercivity value of bulk Ni (ca. 100 Oe)[33] and that of hollow Ni nanometer spheres (ca. 102 Oe),[14b] dandelion-like (ca. 130 Oe),[20a] or flower-like (ca. 173 Oe)[18] Ni nanostructures at room temperature, the chain-like Ni architectures consisting of urchin-like nanostructures exhibit an enhanced value. But this value was lower than that of the one-dimensional nickel nanorods (ca. 264 Oe)[10] or nanobelts (ca. 640 Oe)[10] with high anisotropy. It is well known that the physical and chemical properties of magnetic materials strongly depend on the size, structures, and dimensions of the magnetic particles. The shape of the hysteresis loop may be strongly affected not only by specific particle surface area but also by the magnetic anisotropy.[34] An expression for the magnetostatic energy E_{ms} of the magnetic materials in the shape of a prolate spheroid with semi-major axis c and semi-minor axes of equal length a has been given as follows:[35]

$$E_{ms} = 1/2M^2N_c + 1/2(N_a - N_c)M^2\sin^2\theta \quad (3)$$

where M is the applied magnetic field, θ is the angle of the applied magnetic field to c, N_a and N_c are demagnetizing coefficients along a and c, respectively.

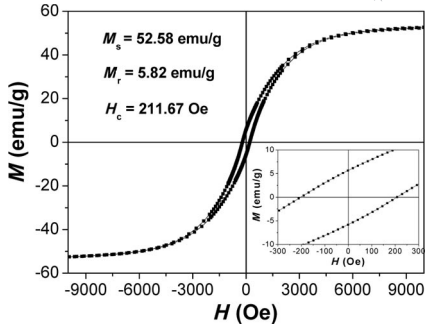

Figure 8. Hysteresis loop for the chain-like Ni architectures assembled from urchin-like hierarchical nanostructures at room temperature.

The shape-anisotropy constant K_s is given by

$$K_s = 1/2(N_a - N_c)M^2 \quad (4)$$

As equation (4) shows, the strength of shape anisotropy depends on the axial ratio c/a of the specimen. Symmetrically shaped nanoparticles, such as spheres, do not have any net shape anisotropy. However, the synthesized representative chain-like Ni architectures with an aspect ratio of about 10 on average would have shape anisotropy, which will increase the coercivity. So, the different coercivity may be attributed to the shape anisotropy of chain-like Ni architectures, which prevent them from magnetizing in directions other than along their easy magnetic axes,[35] hence leading to the enhanced coercivity. As for the saturation magnetization value of the sample, it is found to be little lower than that of the bulk nickel (55 emu/g).[33] This may be due to the spin disorder on the surface and the magnetic interaction between the building blocks, which would reduce the total magnetic moment.[36]

Conclusions

Magnetic metallic Ni chain-like architectures assembled from urchin-like hierarchical nanostructures have been successfully prepared by a simple hydrothermal reduction process without any template or surfactant. The urchin-like nanostructures are composed of dozens of well-aligned metallic Ni sword-like nanopetals growing radially from the surfaces of the spherical particles. A growth mechanism for the formation of self-assembled chain-like architectures assembled from urchin-like hierarchical nanostructures has been proposed. A significantly enhanced magnetic coercivity has been observed for the magnetic Ni chain-like architectures compared to the bulk metal Ni. The present hydrothermal route can be easily controlled. Hence it can be extended to the preparation of complex hierarchical structures from other metals, alloys, or compounds.

Experimental Section

All reagents were of analytic grade and used without further purification. In a typical experiment, $NiCl_2 \cdot 6H_2O$ (0.72 g) was dissolved in deionized water (30 mL) by intensive stirring for 2 h, and a

homogeneous green solution was obtained. An ethanol solution (10 mL) of EDA was added dropwise into an aqueous solution of $NiCl_2 \cdot 6H_2O$ (30 mL) to give a mauve pellucid solution. Then the desired NaOH solution and hydrated hydrazine (3.0 mL, 80%) was added. The whole mixture was transferred into a Teflon cup in a stainless steel-lined autoclave (50 mL capacity), sealed, and maintained at 115 °C for 4 h. After the heat treatment, the black fluffy particles floating on the solution were collected, rinsed with distilled water and absolute ethanol, and finally vacuum-dried at 60 °C.

The phase purity of the products was examined by XRD with a Rigaku D/max 2500 diffractometer at a voltage of 40 kV and a current of 200 mA with Cu-K_α radiation (λ = 1.5406 Å), employing a scanning rate of 0.02°/s in the 2θ range from 20 to 80°. SEM images and EDX analyses were obtained with a HITACHI S-4800 microscope (Japan). TGA-DSC analyses were carried out with a NETZSCH STA-409 PC thermal analyzer with a heating rate of 10 °C min^{-1} in flowing oxygen. TEM images and the corresponding SAED pattern were taken with a Hitachi-600 transmission electron microscope at an accelerating voltage of 200 kV. HRTEM images were recorded with a JEOL JEM-2010 transmission electron microscope at an accelerating voltage of 200 kV. The FTIR spectrum was recorded with a Varian 3100 FTIR spectrometer by using a KBr wafer. Magnetic measurements for the samples were carried out at room temperature by using a vibrating sample magnetometer (VSM, Lakeshore 7307, USA) with a maximum magnetic field of 10 kOe.

Acknowledgments

This work is supported by the Overseas Outstanding Scholar Foundation of the Chinese Academy of Sciences (Grant Nos.: 2005-1-3 and 2005-2-1), the Specialized Research Fund for Outstanding Young Teachers in Shanghai Higher Education Institutions (Grant No.: egd08013), and the Innovation Program of the Shanghai Municipal Education Commission (Grant No.: 10YZ200). We also thank Prof. Shao-Yun Fu for helpful discussions.

[1] J. Chen, D. H. Bradhurst, S. X. Dou, H. K. Liu, *J. Electrochem. Soc.* **1999**, *146*, 3606–3612.
[2] H. G. Yang, H. C. Zeng, *Angew. Chem. Int. Ed.* **2004**, *43*, 5930–5933.
[3] a) G. Kaltenpoth, M. Himmelhaus, L. Slansky, F. Caruso, M. Grunze, *Adv. Mater.* **2003**, *15*, 1113–1118; b) Y. Hou, H. Kondoh, T. Ohta, *Chem. Mater.* **2005**, *17*, 3994–3996; c) L. P. Zhu, H. M. Xiao, W. D. Zhang, Y. Yang, S. Y. Fu, *Cryst. Growth Des.* **2008**, *8*, 1113–1117; d) L. P. Zhu, W. D. Zhang, H. M. Xiao, Y. Yang, S. Y. Fu, *J. Phys. Chem. C* **2008**, *112*, 10073–10078; e) Y. J. Zhang, Q. Yao, Y. Zhang, T. Cui, D. Li, W. Liu, Z. Zhang, *Cryst. Growth Des.* **2008**, *8*, 3206–3212.
[4] a) J. Yuan, K. Laubernds, Q. Zhang, S. L. Suib, *J. Am. Chem. Soc.* **2003**, *125*, 4966–4967; b) M. Yada, C. Taniguchi, T. Torikai, T. Watari, S. Furuta, H. Katsuki, *Adv. Mater.* **2004**, *16*, 1448–1453; c) H. Y. Fan, K. Yang, D. M. Boye, T. Sigmon, K. J. Malloy, H. Xu, G. P. López, C. J. Brinker, *Science* **2004**, *304*, 567–571; d) P. Gao, Z. Wang, *J. Am. Chem. Soc.* **2003**, *125*, 11299–11300; e) J. Hu, L. Ren, Y. Guo, H. Liang, A. Cao, L. Wan, C. Bai, *Angew. Chem. Int. Ed.* **2005**, *44*, 1269–1273; f) L. P. Zhu, H. M. Xiao, X. M. Liu, S. Y. Fu, *J. Mater. Chem.* **2006**, *16*, 1794–1797; g) L. P. Zhu, H. M. Xiao, S. Y. Fu, *Cryst. Growth Des.* **2007**, *7*, 177–182.
[5] a) S. A. Jenekhe, X. L. Chen, *Science* **1998**, *279*, 1903–1907; b) O. Ikkala, G. T. Brinke, *Science* **2002**, *295*, 2407–2409.
[6] J. Du, Y. Chen, *Angew. Chem. Int. Ed.* **2004**, *43*, 5084–5890.
[7] W. Shenton, D. Pum, U. B. Sleytr, S. Mann, *Nature* **1997**, *389*, 585–587.
[8] J. Park, E. Kang, S. U. Son, H. M. Park, M. K. Lee, J. Kim, K. W. Kim, H. J. Noh, J. H. Park, C. J. Bae, J. G. Park, T. Hyeon, *Adv. Mater.* **2005**, *17*, 429–434.
[9] N. Cordente, M. Respaud, F. Senocq, M. J. Casanove, C. Amiens, B. Chaudret, *Nano Lett.* **2001**, *1*, 565–568.
[10] D. E. Zhang, X. M. Ni, H. G. Zheng, T. Y. Li, X. J. Zhang, Z. P. Yang, *Mater. Lett.* **2005**, *59*, 2011–2014.
[11] C. M. Liu, L. Guo, R. M. Wang, Y. Deng, H. B. Xu, S. Yang, *Chem. Commun.* **2004**, 2726–.
[12] Z. Liu, S. Li, Y. Yang, S. Peng, Z. Hu, Y. Qian, *Adv. Mater.* **2003**, *15*, 1946–1948.
[13] J. C. Bao, C. Y. Tie, Z. Xu, Q. F. Zhou, D. Shen, Q. Ma, *Adv. Mater.* **2001**, *13*, 1631–1633.
[14] a) J. C. Bao, Y. Liang, Z. Xu, L. Si, *Adv. Mater.* **2003**, *15*, 1832–1835; b) Q. Liu, H. Liu, M. Han, J. Zhu, Y. Liang, Z. Xu, Y. Song, *Adv. Mater.* **2005**, *17*, 1995–1999; c) Y. Wang, Q. Zhu, H. Zhang, *J. Mater. Chem.* **2006**, *16*, 1212–1214.
[15] X. Ni, J. Zhang, Y. Zhang, H. Zheng, *J. Colloid Interface Sci.* **2007**, *307*, 554–558.
[16] H. Wu, R. Zhang, X. Liu, D. Lin, W. Pan, *Chem. Mater.* **2007**, *19*, 3506–3511.
[17] Y. Leng, Y. Wang, X. Li, T. Liu, S. Takahashhi, *Nanotechnology* **2006**, *17*, 4834–4839.
[18] X. Ni, Q. Zhao, H. Zheng, B. Li, J. Song, D. Zhang, X. Zhang, *Eur. J. Inorg. Chem.* **2005**, 4788–4793.
[19] X. M. Liu, S. Y. Fu, *J. Cryst. Growth* **2007**, *306*, 428–432.
[20] a) J. T. Tian, C. H. Gong, L. G. Yu, Z. S. Wu, Z. J. Zhang, *Chin. Chem. Lett.* **2008**, *19*, 1123–1126; b) F. Ma, Q. Li, J. Huang, J. Li, *J. Cryst. Growth* **2008**, *310*, 3522–3526.
[21] L. P. Zhu, H. M. Xiao, S. Y. Fu, *Eur. J. Inorg. Chem.* **2007**, 3947–3951.
[22] L. P. Zhu, W. D. Zhang, H. M. Xiao, G. Yang, S. Y. Fu, *Cryst. Growth Des.* **2008**, *8*, 957–963.
[23] M. Wen, Y. F. Wang, F. Zhang, Q. S. Wu, *J. Phys. Chem. C* **2009**, *113*, 5960–5966.
[24] L. H. Zhang, H. Q. Yang, J. Yu, F. H. Shao, L. Li, F. H. Zhang, H. Zhao, *J. Phys. Chem. C* **2009**, *113*, 5434–5443.
[25] M. R. Kim, D. J. Jang, *Chem. Commun.* **2008**, 5218–5220.
[26] X. J. Wang, K. Han, F. Q. Wan, Y. J. Gao, K. Jiang, *Mater. Lett.* **2008**, *62*, 3509–3511.
[27] H. Tang, J. G. Yu, X. F. Zhao, *J. Alloys Compd.* **2008**, *460*, 513–518.
[28] U. Pal, P. Santiago, *J. Phys. Chem. B* **2005**, *109*, 15317–15321.
[29] Y. C. Zhang, G. Y. Wang, X. Y. Hu, R. Xing, *J. Solid State Chem.* **2005**, *178*, 1609–1613.
[30] H. P. Klug, L. E. Alexander, *X-ray Diffraction Procedure*, 2nd ed., Wiley, New York, **1974**.
[31] C. Pacholski, A. Kornowski, H. Weller, *Angew. Chem. Int. Ed.* **2002**, *41*, 1188–1191.
[32] V. Salgueirino-Maceira, M. A. Correa-Duarte, A. Hucht, M. Farle, *J. Magn. Magn. Mater.* **2006**, *303*, 163–166.
[33] W. Gong, H. Li, Z. Zhao, J. Chen, *J. Appl. Phys.* **1991**, *69*, 5119–5121.
[34] B. D. Cullity (Ed.), *Introduction to Magnetic Materials*, Addison-Wesley, London, **1972**, pp. 240–245.
[35] J. Wang, Q. W. Chen, C. Zeng, B. Y. Hou, *Adv. Mater.* **2004**, *16*, 137–140.
[36] S. H. Wu, D. H. Chen, *J. Colloid Interface Sci.* **2003**, *259*, 282–286.

Received: September 7, 2009
Published Online: February 2, 2010

